Research Article | Vol. 7, No. 11 | 1 Nov 2016 | BIOMEDICAL OPTICS EXPRESS 4364

Biomedical Optics EXPRESS

Optical redox ratio identifies metastatic potential-dependent changes in breast cancer cell metabolism

KINAN ALHALLAK, LISA G. REBELLO, TIMOTHY J. MULDOON, KYLE P. QUINN, AND NARASIMHAN RAJARAM*

Department of Biomedical Engineering, University of Arkansas, Fayetteville, AR 72701, USA
**nrajaram@uark.edu*

Abstract: The development of prognostic indicators of breast cancer metastatic risk could reduce the number of patients receiving chemotherapy for tumors with low metastatic potential. Recent evidence points to a critical role for cell metabolism in driving breast cancer metastasis. Endogenous fluorescence intensity of nicotinamide adenine dinucleotide (NADH) and flavin adenine dinucleotide (FAD) can provide a label-free method for assessing cell metabolism. We report the optical redox ratio of FAD/(FAD + NADH) of four isogenic triple-negative breast cancer cell lines with varying metastatic potential. Under normoxic conditions, the redox ratio increases with increasing metastatic potential (168FARN>4T07>4T1), indicating a shift to more oxidative metabolism in cells capable of metastasis. Reoxygenation following acute hypoxia increased the redox ratio by 43 ± 9% and 33 ± 4% in the 4T1 and 4T07 cells, respectively; in contrast, the redox ratio decreased 14 ± 7% in the non-metastatic 67NR cell line. These results demonstrate that the optical redox ratio is sensitive to the metabolic adaptability of breast cancer cells with high metastatic potential and could potentially be used to measure dynamic functional changes that are indicative of invasive or metastatic potential.

OCIS codes: (170.1530) Cell analysis; (170.2520) Fluorescence microscopy; (170.2655) Functional monitoring and imaging

References and links

1. N. L. Henry, M. R. Somerfield, V. G. Abramson, K. H. Allison, C. K. Anders, D. T. Chingos, A. Hurria, T. H. Openshaw, and I. E. Krop, "Role of Patient and Disease Factors in Adjuvant Systemic Therapy Decision Making for Early-Stage, Operable Breast Cancer: American Society of Clinical Oncology Endorsement of Cancer Care Ontario Guideline Recommendations," J. Clin. Oncol. **34**(19), 2303–2311 (2016).
2. R. Peto, C. Davies, J. Godwin, R. Gray, H. C. Pan, M. Clarke, D. Cutter, S. Darby, P. McGale, C. Taylor, Y. C. Wang, J. Bergh, A. Di Leo, K. Albain, S. Swain, M. Piccart, and K. Pritchard; Early Breast Cancer Trialists' Collaborative Group (EBCTCG), "Comparisons between different polychemotherapy regimens for early breast cancer: meta-analyses of long-term outcome among 100,000 women in 123 randomised trials," Lancet **379**(9814), 432–444 (2012).
3. M. Cronin, C. Sangli, M.-L. Liu, M. Pho, D. Dutta, A. Nguyen, J. Jeong, J. Wu, K. C. Langone, and D. Watson, "Analytical Validation of the Oncotype DX Genomic Diagnostic Test for Recurrence Prognosis and Therapeutic Response Prediction in Node-Negative, Estrogen Receptor-Positive Breast Cancer," Clin. Chem. **53**(6), 1084–1091 (2007).
4. O. Warburg, K. Posener, and E. Negelein, "The metabolism of the carcinoma cell," The Metabolism of Tumors. New York, Richard R. Smith, Inc, 29169 (1931).
5. X. Lin, F. Zhang, C. M. Bradbury, A. Kaushal, L. Li, D. R. Spitz, R. L. Aft, and D. Gius, "2-Deoxy-D-glucose-induced cytotoxicity and radiosensitization in tumor cells is mediated via disruptions in thiol metabolism," Cancer Res. **63**(12), 3413–3417 (2003).
6. C. Groussard, I. Morel, M. Chevanne, M. Monnier, J. Cillard, and A. Delamarche, "Free radical scavenging and antioxidant effects of lactate ion: an in vitro study," J. Appl. Physiol. **89**(1), 169–175 (2000).
7. C. Ruckenstuhl, S. Büttner, D. Carmona-Gutierrez, T. Eisenberg, G. Kroemer, S. J. Sigrist, K.-U. Fröhlich, and F. Madeo, "The Warburg Effect Suppresses Oxidative Stress Induced Apoptosis in a Yeast Model for Cancer," PLoS One **4**(2), e4592 (2009).
8. X. Lu, B. Bennet, E. Mu, J. Rabinowitz, and Y. Kang, "Metabolomic changes accompanying transformation and acquisition of metastatic potential in a syngeneic mouse mammary tumor model," J. Biol. Chem. **285**(13), 9317–9321 (2010).

#270141 http://dx.doi.org/10.1364/BOE.7.004364
Journal © 2016 Received 5 Aug 2016; revised 16 Sep 2016; accepted 29 Sep 2016; published 3 Oct 2016

Biomedical Optics EXPRESS

9. P. E. Porporato, V. L. Payen, J. Pérez-Escuredo, C. J. De Saedeleer, P. Danhier, T. Copetti, S. Dhup, M. Tardy, T. Vazeille, C. Bouzin, O. Feron, C. Michiels, B. Gallez, and P. Sonveaux, "A Mitochondrial Switch Promotes Tumor Metastasis," Cell Reports **8**(3), 754–766 (2014).
10. V. S. LeBleu, J. T. O'Connell, K. N. Gonzalez Herrera, H. Wikman, K. Pantel, M. C. Haigis, F. M. de Carvalho, A. Damascena, L. T. Domingos Chinen, R. M. Rocha, J. M. Asara, and R. Kalluri, "PGC-1α mediates mitochondrial biogenesis and oxidative phosphorylation in cancer cells to promote metastasis," Nat. Cell Biol. **16**(10), 992–1003 (2014).
11. F. Dupuy, S. Tabariès, S. Andrzejewski, Z. Dong, J. Blagih, M. G. Annis, A. Omeroglu, D. Gao, S. Leung, E. Amir, M. Clemons, A. Aguilar-Mahecha, M. Basik, E. E. Vincent, J. St-Pierre, R. G. Jones, and P. M. Siegel, "PDK1-dependent metabolic reprogramming dictates metastatic potential in breast cancer," Cell Metab. **22**(4), 577–589 (2015).
12. B. Chance, P. Cohen, F. Jobsis, and B. Schoener, "Intracellular oxidation-reduction states in vivo," Science **137**(3529), 499–508 (1962).
13. B. Chance, B. Schoener, R. Oshino, F. Itshak, and Y. Nakase, "Oxidation-reduction ratio studies of mitochondria in freeze-trapped samples. NADH and flavoprotein fluorescence signals," J. Biol. Chem. **254**(11), 4764–4771 (1979).
14. K. P. Quinn, G. V. Sridharan, R. S. Hayden, D. L. Kaplan, K. Lee, and I. Georgakoudi, "Quantitative metabolic imaging using endogenous fluorescence to detect stem cell differentiation," Sci. Rep. **3**, 3432 (2013).
15. K. P. Quinn, E. Bellas, N. Fourligas, K. Lee, D. L. Kaplan, and I. Georgakoudi, "Characterization of metabolic changes associated with the functional development of 3D engineered tissues by non-invasive, dynamic measurement of individual cell redox ratios," Biomaterials **33**(21), 5341–5348 (2012).
16. N. Ramanujam, R. Richards-Kortum, S. Thomsen, A. Mahadevan-Jansen, M. Follen, and B. Chance, "Low temperature fluorescence imaging of freeze-trapped human cervical tissues," Opt. Express **8**(6), 335–343 (2001).
17. R. Drezek, C. Brookner, I. Pavlova, I. Boiko, A. Malpica, R. Lotan, M. Follen, and R. Richards-Kortum, "Autofluorescence Microscopy of Fresh Cervical-Tissue Sections Reveals Alterations in Tissue Biochemistry with Dysplasia," Photochem. Photobiol. **73**(6), 636–641 (2001).
18. M. C. Skala, J. M. Squirrell, K. M. Vrotsos, J. C. Eickhoff, A. Gendron-Fitzpatrick, K. W. Eliceiri, and N. Ramanujam, "Multiphoton microscopy of endogenous fluorescence differentiates normal, precancerous, and cancerous squamous epithelial tissues," Cancer Res. **65**(4), 1180–1186 (2005).
19. M. C. Skala, K. M. Riching, A. Gendron-Fitzpatrick, J. Eickhoff, K. W. Eliceiri, J. G. White, and N. Ramanujam, "In vivo multiphoton microscopy of NADH and FAD redox states, fluorescence lifetimes, and cellular morphology in precancerous epithelia," Proc. Natl. Acad. Sci. U.S.A. **104**(49), 19494–19499 (2007).
20. A. Varone, J. Xylas, K. P. Quinn, D. Pouli, G. Sridharan, M. E. McLaughlin-Drubin, C. Alonzo, K. Lee, K. Münger, and I. Georgakoudi, "Endogenous Two-Photon Fluorescence Imaging Elucidates Metabolic Changes Related to Enhanced Glycolysis and Glutamine Consumption in Precancerous Epithelial Tissues," Cancer Res. **74**(11), 3067–3075 (2014).
21. J. H. Ostrander, C. M. McMahon, S. Lem, S. R. Millon, J. Q. Brown, V. L. Seewaldt, and N. Ramanujam, "Optical Redox Ratio Differentiates Breast Cancer Cell Lines Based on Estrogen Receptor Status," Cancer Res. **70**(11), 4759–4766 (2010).
22. A. Walsh, R. S. Cook, B. Rexer, C. L. Arteaga, and M. C. Skala, "Optical imaging of metabolism in HER2 overexpressing breast cancer cells," Biomed. Opt. Express **3**(1), 75–85 (2012).
23. A. J. Walsh, R. S. Cook, H. C. Manning, D. J. Hicks, A. Lafontant, C. L. Arteaga, and M. C. Skala, "Optical Metabolic Imaging Identifies Glycolytic Levels, Subtypes, and Early-Treatment Response in Breast Cancer," Cancer Res. **73**(20), 6164–6174 (2013).
24. A. T. Shah, M. Demory Beckler, A. J. Walsh, W. P. Jones, P. R. Pohlmann, and M. C. Skala, "Optical Metabolic Imaging of Treatment Response in Human Head and Neck Squamous Cell Carcinoma," PLoS One **9**(3), e90746 (2014).
25. A. J. Walsh, R. S. Cook, M. E. Sanders, L. Aurisicchio, G. Ciliberto, C. L. Arteaga, and M. C. Skala, "Quantitative Optical Imaging of Primary Tumor Organoid Metabolism Predicts Drug Response in Breast Cancer," Cancer Res. **74**(18), 5184–5194 (2014).
26. H. N. Xu, S. Nioka, J. D. Glickson, B. Chance, and L. Z. Li, "Quantitative mitochondrial redox imaging of breast cancer metastatic potential," J. Biomed. Opt. **15**, 036010 (2010).
27. C. J. Aslakson and F. R. Miller, "Selective events in the metastatic process defined by analysis of the sequential dissemination of subpopulations of a mouse mammary tumor," Cancer Res. **52**(6), 1399–1405 (1992).
28. J. Yang, S. A. Mani, J. L. Donaher, S. Ramaswamy, R. A. Itzykson, C. Come, P. Savagner, I. Gitelman, A. Richardson, and R. A. Weinberg, "Twist, a master regulator of morphogenesis, plays an essential role in tumor metastasis," Cell **117**(7), 927–939 (2004).
29. R. V. Simões, I. S. Serganova, N. Kruchevsky, A. Leftin, A. A. Shestov, H. T. Thaler, G. Sukenick, J. W. Locasale, R. G. Blasberg, J. A. Koutcher, and E. Ackerstaff, "Metabolic plasticity of metastatic breast cancer cells: adaptation to changes in the microenvironment," Neoplasia **17**(8), 671–684 (2015).
30. B. P. Dranka, G. A. Benavides, A. R. Diers, S. Giordano, B. R. Zelickson, C. Reily, L. Zou, J. C. Chatham, B. G. Hill, J. Zhang, A. Landar, and V. M. Darley-Usmar, "Assessing bioenergetic function in response to oxidative stress by metabolic profiling," Free Radic. Biol. Med. **51**(9), 1621–1635 (2011).
31. M. Skala and N. Ramanujam, "Multiphoton redox ratio imaging for metabolic monitoring in vivo," in *Advanced Protocols in Oxidative Stress II* (Springer, 2010), pp. 155–162.

Biomedical Optics EXPRESS

32. J. Hou, H. J. Wright, N. Chan, R. Tran, O. V. Razorenova, E. O. Potma, and B. J. Tromberg, "Correlating two-photon excited fluorescence imaging of breast cancer cellular redox state with seahorse flux analysis of normalized cellular oxygen consumption," J. Biomed. Opt. **21**(6), 060503 (2016).
33. Y. Dai, K. Bae, and D. W. Siemann, "Impact of hypoxia on the metastatic potential of human prostate cancer cells," Int. J. Radiat. Oncol. Biol. Phys. **81**(2), 521–528 (2011).
34. A. J. Walsh and M. C. Skala, "Optical metabolic imaging quantifies heterogeneous cell populations," Biomed. Opt. Express **6**(2), 559–573 (2015).
35. A. J. Walsh, J. A. Castellanos, N. S. Nagathihalli, N. B. Merchant, and M. C. Skala, "Optical Imaging of Drug-Induced Metabolism Changes in Murine and Human Pancreatic Cancer Organoids Reveals Heterogeneous Drug Response," Pancreas **45**(6), 863–869 (2016).
36. L. Z. Li, R. Zhou, H. N. Xu, L. Moon, T. Zhong, E. J. Kim, H. Qiao, R. Reddy, D. Leeper, B. Chance, and J. D. Glickson, "Quantitative magnetic resonance and optical imaging biomarkers of melanoma metastatic potential," Proc. Natl. Acad. Sci. U.S.A. **106**(16), 6608–6613 (2009).
37. W. S. Kunz and W. Kunz, "Contribution of different enzymes to flavoprotein fluorescence of isolated rat liver mitochondria," Biochimica et Biophysica Acta (BBA)- General Subjects **841**(3), 237–246 (1985).
38. G. L. Wang, B. H. Jiang, E. A. Rue, and G. L. Semenza, "Hypoxia-inducible factor 1 is a basic-helix-loop-helix-PAS heterodimer regulated by cellular O2 tension," Proc. Natl. Acad. Sci. U.S.A. **92**(12), 5510–5514 (1995).
39. D. J. Chaplin, P. L. Olive, and R. E. Durand, "Intermittent blood flow in a murine tumor: radiobiological effects," Cancer Res. **47**(2), 597–601 (1987).
40. H. Kimura, R. D. Braun, E. T. Ong, R. Hsu, T. W. Secomb, D. Papahadjopoulos, K. Hong, and M. W. Dewhirst, "Fluctuations in red cell flux in tumor microvessels can lead to transient hypoxia and reoxygenation in tumor parenchyma," Cancer Res. **56**(23), 5522–5528 (1996).
41. J. Lanzen, R. D. Braun, B. Klitzman, D. Brizel, T. W. Secomb, and M. W. Dewhirst, "Direct demonstration of instabilities in oxygen concentrations within the extravascular compartment of an experimental tumor," Cancer Res. **66**(4), 2219–2223 (2006).
42. E. Louie, S. Nik, J. S. Chen, M. Schmidt, B. Song, C. Pacson, X. F. Chen, S. Park, J. Ju, and E. I. Chen, "Identification of a stem-like cell population by exposing metastatic breast cancer cell lines to repetitive cycles of hypoxia and reoxygenation," Breast Cancer Res. **12**(6), R94 (2010).
43. R. A. Cairns and R. P. Hill, "Acute hypoxia enhances spontaneous lymph node metastasis in an orthotopic murine model of human cervical carcinoma," Cancer Res. **64**(6), 2054–2061 (2004).
44. R. A. Cairns, T. Kalliomaki, and R. P. Hill, "Acute (cyclic) hypoxia enhances spontaneous metastasis of KHT murine tumors," Cancer Res. **61**(24), 8903–8908 (2001).
45. R. Boidot, S. Branders, T. Helleputte, L. I. Rubio, P. Dupont, and O. Feron, "A generic cycling hypoxia-derived prognostic gene signature: application to breast cancer profiling," Oncotarget **5**(16), 6947–6963 (2014).
46. R. Sepehr, K. Staniszewski, S. Maleki, E. R. Jacobs, S. Audi, and M. Ranji, "Optical imaging of tissue mitochondrial redox state in intact rat lungs in two models of pulmonary oxidative stress," J. Biomed. Opt. **17**(4), 046010 (2012).
47. C. Lehuédé, F. Dupuy, R. Rabinovitch, R. G. Jones, and P. M. Siegel, "Metabolic Plasticity as a Determinant of Tumor Growth and Metastasis," Cancer Res. **76**(18), 5201–5208 (2016).

1. Introduction

About 90% of breast cancer patients die due to metastatic spread and not due to the primary tumor. Clinically established prognostic indicators of metastatic recurrence include lymph node status, tumor stage, progesterone (PgR) and estrogen (ER) receptor status, human epidermal growth factor (HER2/neu), and lymphovascular invasion [1]. Adjuvant chemotherapy reduces the risk of metastatic recurrence by at least 30% [2], and can be of significant benefit in patients classified as high risk based on the previously described prognostic indicators. For early-stage breast cancers with good prognosis (<10% odds of distant recurrence), adjuvant chemotherapy presents no significant benefits over surgery and local radiation alone. However, the morbidity associated with the development of tumor metastases has led to a majority of the 240,000 patients diagnosed annually with breast cancer receiving adjuvant chemotherapy. To reduce the number of patients receiving chemotherapy without significant benefit, American Society for Clinical Oncology (ASCO) guidelines recommend consideration of the Oncotype DX recurrence score. Oncotype DX is a 21-gene expression signature that is highly correlated with distant relapse in hormone receptor-positive, HER2-negative, lymph-node negative breast cancer, and has been approved by the Food and Drug Administration (FDA) [3]. However, the Oncotype DX test is expensive ($4,000/test) and not available at all clinical facilities. Therefore, there is a need to develop cost-effective prognostic indicators that can reduce the number of patients receiving life-altering chemotherapy for early-stage breast cancers with very low recurrence risk.

Biomedical Optics EXPRESS

One of the most important changes in the early tumor microenvironment that fuels tumor growth is metabolic reprogramming. Otto Warburg discovered, nearly 80 years ago, that cancer cells preferentially metabolize glucose to lactate even in the presence of oxygen, and use glycolysis instead of oxidative phosphorylation to meet their energy needs [4]. This phenomenon – aerobic glycolysis – has been shown to provide cancer cells with a significant growth advantage by avoiding mitochondrial reactive oxygen species (ROS), generating biomass for cell proliferation through the pentose phosphate pathway, and replenishing of ROS scavengers to decrease ROS-induced cell death [5–7]. Recent studies have shown that although this switch to aerobic glycolysis might be useful for rapid cell proliferation and tumor growth, highly invasive and metastatic cancer cells may favor mitochondrial oxidative metabolism to efficiently generate ATP and promote a migratory phenotype [8–10]. Furthermore, metastatic cancer cells were shown to utilize glycolysis or oxidative phosphorylation depending on their site of metastasis [11]. These studies demonstrate that knowledge of the specific metabolic pathway utilized by breast cancer cells could play an important role in determining their invasive and migratory tendencies.

Optical imaging of the endogenous fluorescence of nicotinamide adenine dinucleotide (NADH) and flavin adenine dinucleotide (FAD) presents a non-destructive and label-free method for assessing cell metabolism [12]. NADH and FAD are metabolic cofactors that play a critical role in the generation of ATP through oxidative phosphorylation. Within the mitochondria, oxidation of NADH to NAD^+ and $FADH_2$ to FAD at complexes I and II (electron transport chain), respectively leads to the donation of electrons to molecular oxygen. Because only the NADH and FAD forms are fluorescent, measuring the ratio of FAD/(FAD + NADH) can be used to measure cell redox state (henceforth referred to as optical redox ratio) [13]. Changes in the redox ratio of a cell can be interpreted as a relative change in the rate of glucose catabolism to oxidative phosphorylation. During oxidative phosphorylation, NADH fluorescence decreases due to conversion to non-fluorescent NAD^+, and FAD fluorescence increases due to its generation from non-fluorescent $FADH_2$, leading to an increase in the redox ratio. The absence of oxygen or a need to increase glucose catabolism leads to a build-up of NADH that does not get converted to NAD^+, causing an increase in NADH fluorescence and a decrease in the redox ratio. The redox ratio is strongly associated with the concentrations of NAD^+/NADH [14], and has been used *in vitro* and *in vivo* to track metabolic changes during cell differentiation [14, 15] and malignant transformation [16–20]. The optical redox ratio has been shown to be sensitive to ER status and HER2 expression in breast cancer cells [21, 22] as well as therapy-induced changes in cellular metabolism [23–25]. Although studies have identified significant differences in redox ratio of benign and aggressive human breast cancer cells with different receptor status [21, 26], no study has investigated changes in the optical redox ratio within a model of metastatic cancer progression.

The goal of this study was to determine the sensitivity of the optical redox ratio to changes in cellular metabolism in cell lines that occupy the complete spectrum of metastatic progression. We measured the optical redox ratio in a panel of isogenic breast cancer lines – 4T1, 4T07, 168FARN, and 67NR – that were derived from a single spontaneous murine breast tumor. The 4T1 panel of breast cancer cells presents a unique model of metastatic cancer progression because each cell line is only capable of completing specific steps in the metastatic process (primary tumor formation, invasion, intravasation, extravasation, metastatic node formation) [11, 27, 28]. We initially determined the sensitivity of the optical redox ratio to dynamic changes in oxygen consumption and validated these measurements using a commercially available metabolic assay. The redox ratio of each cell line was measured under normoxic conditions and upon reoxygenation following acute hypoxia. Our results demonstrate significant differences in redox ratio between the different breast cancer cell lines and cell line-specific changes in the metabolic response to acute hypoxia.

Biomedical Optics EXPRESS

2. Methods

2.1 Cell culture

The cell lines used in this study – 4T1, 4T07, 168FARN, and 67NR – were originally derived from a spontaneous breast tumor growing in a Balb/c mouse [27], and were kindly provided by Dr. Fred Miller (Karmanos Cancer Institute). All four cell lines are triple-negative (ER-, HER2-, and PgR-). Cells were cultured in Dulbecco's Modified Eagle's Medium (DMEM) with the addition of 10% (v/v) fetal bovine serum (FBS), 2 mM L-glutamine, 1% (v/v) nonessential amino acids, and 1% (v/v) penicillin-streptomycin. The cells were cultured in a humidified incubator set to 5% CO_2 and 37°C and passaged when they reached approximately 80% confluence. Cells were used within the first 10 passages for all experiments.

2.2 Exposure to acute hypoxia

A dual gas controller (Oxycycler C42, Biospherix, Parish, NY) connected to a modular sub-chamber was used to control oxygen, nitrogen, and carbon dioxide levels. The sub-chamber can hold several cell plates, and is placed within a regular incubator. The gas controller is placed outside the incubator and communicates with the sub-chamber through an access port in the door of the incubator. The gas controller was set to a constant level of 0.5% O_2 and 5% CO_2 for a period of 60 minutes. The controller reaches the set point of 0.5% O_2 in approximately 15-20 minutes. The hypoxic exposure of cells for 60 minutes commenced after the chamber had reached the desired set point.

2.3 Seahorse metabolic flux assay

A Seahorse XFp extracellular flux analyzer (Seahorse Biosciences, Santa Clara, CA) was used to establish the mitochondrial and glycolytic function of the cells under normoxic and post-hypoxic conditions. Each XFp miniplate consists of 8 wells – 2 background and 6 sample. The size of each well is comparable to the well size in a 96-well plate. Cell densities were optimized based on cell size to ensure that cells were not over-confluent after 24 hours. 4T1, 4T07, 168FARN, and 67NR were plated at a density of 7500, 10000, 12500, and 15000 cells per well, respectively. A separate 96-well plate with the same number of plated cells was used to determine cell count at the time of the experiment for the purpose of normalizing the data, as performed in previous studies [29]. Cell plates were placed in a CO_2 incubator and allowed to grow for 24 hours. After 24 hours, the original media in the cell plates was replaced with Seahorse assay media, and the cells were placed in a non-CO_2 incubator at 37°C for 60 minutes prior to the start of the assay. This is done to remove any CO_2 from plates to ensure accurate pH measurements. To calculate oxygen consumption rate (OCR) and proton production rate (PPR), three compounds are added sequentially to perturb mitochondrial respiration [30]–oligomycin (0.2 μM), carbonylcyanide p-triflouromethoxyphenylhydrazone (FCCP; 0.2 μM), and rotenone/antimycin A mixture (RAAM; 0.1 μM). For the hypoxic experiments, the cells were diluted with the assay media immediately after the hypoxic exposure and placed in a non-CO_2 incubator to outgas the CO_2 within the wells. The Seahorse data shown in Fig. 2 represent the basal OCR and PPR values (prior to drug injection). Sequential injection of the drugs provides a host of other readouts (maximal respiration, ATP production, spare respiratory capacity) that are not discussed in this paper.

2.4 Multiphoton imaging of the optical redox ratio

Cells were plated on a glass slide at a density of 2.5 x 10^5 cells per well in a standard 6-well plate on the day prior to the experiment. After 24 hours, the glass slide was removed, placed in a heated chamber (37°C) and perfused with 2 ml of glucose-free media (for the normoxia and post-hypoxia experiments shown in Fig. 2). However, these studies can also be performed using regular medium. Given that imaging is performed within 5-10 minutes of removal from

Biomedical Optics EXPRESS

the incubator, we do not expect any changes in the redox ratio due to use of glucose-free media. The mitochondrial perturbation experiments (Fig. 1) used the same media and conditions as the Seahorse assay. Imaging was performed using a custom-built resonant-scanning multiphoton microscope with a MaiTai ultrafast Ti:Sapphire tunable laser source (Spectra-Physics, Santa Clara CA). The laser excitation source was tuned to 755 nm (NADH fluorescence) or 860 nm (FAD fluorescence), and images were acquired via non-descanned GaAsP photomultipler tubes (H7422-40, Hamamatsu) with 460/40 nm (NADH) or 525/40 nm (FAD) bandpass filters, respectively. Images (512 x 512 pixels; 16-bit depth; 130 μm x 130 μm) were acquired using a 40x water immersion objective (NA = 0.8, working distance = 3.5 mm, diffraction-limited lateral resolution = 0.6 μm). Rhodamine measurements were acquired at the end of each experiment for calibration [31]. To assess the dynamic response of redox ratio to changes in oxygen consumption, NADH and FAD fluorescence was measured continuously with serial addition of drugs. A separate control plate was imaged to determine non-specific changes in endogenous fluorescence over the same time interval. Image analysis was performed using MATLAB.

Redox images were created by computing pixel-wise ratios of FAD/(NADH + FAD) fluorescence. For statistical analysis and bar plot presentation, the average redox ratios of cell plates were calculated by separately computing the average FAD and NADH intensities from the respective images and taking the ratio of these values. For each cell line, 3 separate cell plates were imaged at normoxia and after acute hypoxia. Within each cell plate, 3 fields of view were acquired and 6 cells were randomly selected within each field of view. Two independent runs of these experiments were performed.

2.5 Statistical analysis

A nested, two-way analysis of variance (ANOVA) was used to determine statistical significant differences in the average redox ratio. Breast cancer cell line and the hypoxic perturbation were considered fixed effects while the cell plates and fields of view nested within each group were considered random effects. Interactions between all effects were also considered. Post-hoc Tukey HSD tests were used to evaluate statistical significance between specific cell groups.

3. Results

3.1 Optical redox ratio is sensitive to dynamic changes in oxygen consumption

To evaluate the ability of the optical redox ratio to report on dynamic changes in oxygen consumption, we acquired images corresponding to the fluorescence emission channels of NADH and FAD (Fig. 1(A)) from 4T1 breast cancer cells at baseline (no drug injection) and after sequential addition of 3 mitochondrial inhibitors/uncouplers, similar to the Seahorse metabolic flux assay. The actions of these drugs and their effect on NADH and FAD activity within the mitochondria are illustrated in the Appendix (Fig. 4). Oligomycin inhibits mitochondrial H^+-ATP synthase and decreases cellular respiration. Subsequent addition of FCCP drives mitochondrial consumption of NADH by uncoupling electron transport from ATP generation. Finally, rotenone and antimycin A inhibit electron transport at complexes I and III, respectively. We found that the changes in the average redox ratio in response to these drugs (Fig. 1(B)) were consistent with the expected actions of these drugs and with measurements of the normalized oxygen consumption rate (n-OCR). We calculated n-OCR as the ratio of OCR/PPR. A control plate that received no drugs showed no change in the redox ratio over the same time interval (data not shown). These results establish the sensitivity of the optical redox ratio to dynamic changes in oxygen consumption, and are consistent with a recent study that demonstrated the same using human breast cancer cells [32].

Biomedical Optics EXPRESS

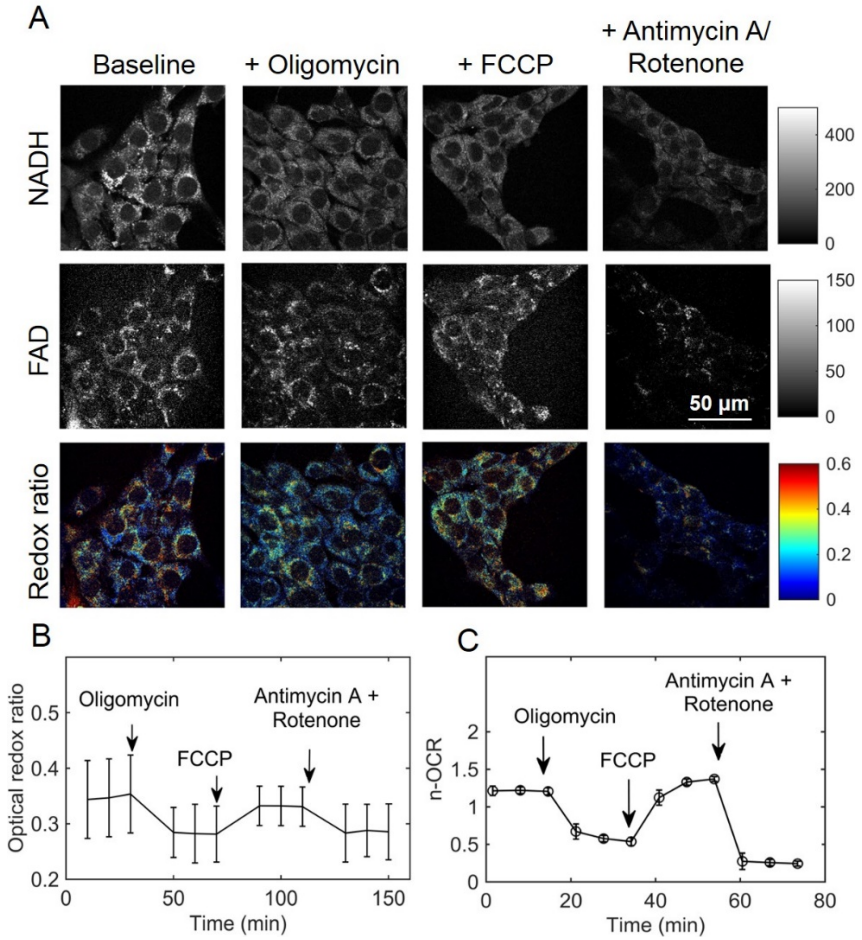

Fig. 1. Optical redox ratio is sensitive to dynamic changes in oxygen consumption. **A.** Representative images of NADH, FAD and the calculated optical redox ratio (FAD/FAD + NADH) in response to the addition of mitochondrial inhibitors and uncouplers. All images were acquired from different fields of view within the same cell plate over several minutes after serial addition of each drug indicated above the figure panels. **B.** Quantification of the dynamic changes in the optical redox ratio in response to serial drug additions. Oligomycin, FCCP, and antimycin A/rotenone were injected at T = 30, 70, and 110 minutes, respectively. **C.** Normalized oxygen consumption rate measured using the Seahorse XFp analyzer. Oligomycin, FCCP, and antimycin A/rotenone were injected at T = 15, 35, and 55 minutes, respectively. The error bars are a standard deviation of the mean plate value.

3.2 Optical redox ratio is significantly different in breast cancer cells of different metastatic potential under normoxic conditions and following reoxygenation from acute hypoxia

We determined the optical redox ratio of each cell line in the murine breast cancer panel (Table 1). Only the 4T1 cell line is capable of completing all the steps necessary to form efficient metastatic nodes in the liver, lung and brain. The 168FARN and 4T07 are considered to be weakly metastatic whereas the 67NR is non-metastatic.

Biomedical Optics EXPRESS

Table 1. Invasion – metastasis cascade for Balb/c tumor-derived breast cancer cell lines

Cell line	Invasion - Metastasis cascade	Metastatic site
67NR	Primary tumor formation only	N/A
168FARN	Primary tumor + local invasion + intravasation	Lymph nodes
4T07	+ Extravasation	Micrometastases in lung, lymph nodes
4T1	+ Metastatic growth	Lung, Liver, Bone

Under baseline, normoxic conditions (21% O_2), the optical redox ratios of all four breast cancer cell lines were significantly different from each other. (Fig. 2(A) and 2(B)). Additionally, there was a trend towards lower redox ratio as we progressed from the highly metastatic 4T1 to the poorly metastatic 168FARN cells (Fig. 2(B)). The non-metastatic 67NR cells had the highest average redox ratio. Because acute hypoxia is capable of eliciting a pro-migratory response [33], we investigated the optical redox ratio of these cell lines after 60 minutes of reoxygenation following acute hypoxia. The average redox ratio of the 4T1 and 4T07 cells (Fig. 2(B)) following reoxygenation was significantly higher compared with their respective normoxic groups ($p < 0.0001$ for both cell lines). We observed a small but statistically insignificant increase in the redox ratio of 168FARN cells ($p = 0.82$). On the other hand, the 67NR showed a significant decrease in redox ratio ($p = 0.008$). The changes in redox ratio after exposure to acute hypoxia within each cell line are consistent with n-OCR data obtained using the Seahorse metabolic assay.

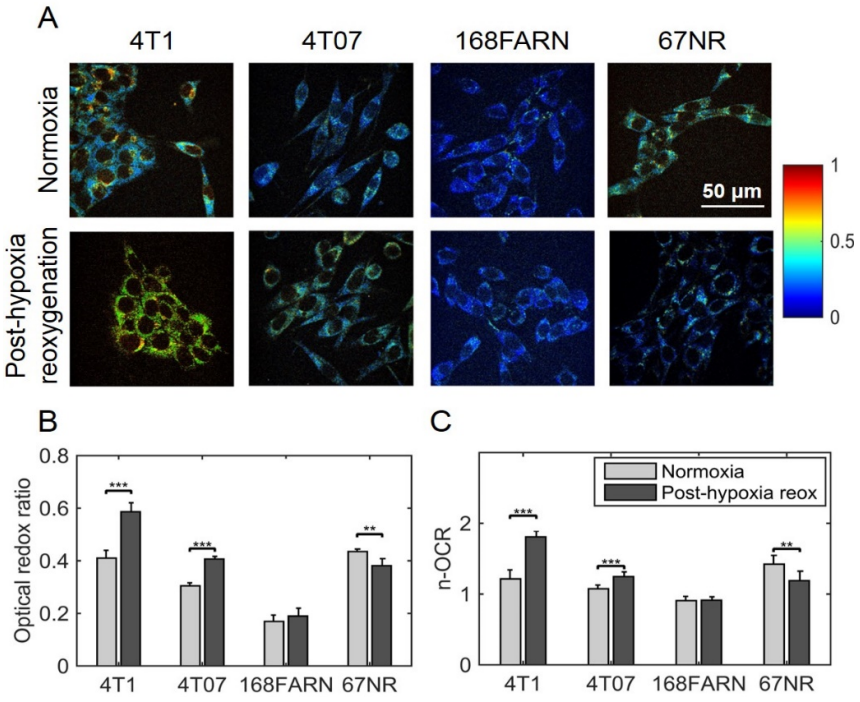

Fig. 2. Optical redox ratio of breast cancer cells of different metastatic potential is significantly different at normoxia and after exposure to acute hypoxia. **A.** Representative redox ratio images for 4T1, 4T07, 168FARN, and 67NR breast cancer cells. The redox ratio was measured at baseline normoxic conditions and 1 hour after exposure to acute hypoxia (60 minutes, 0.5% O_2). **B.** Quantification of redox ratio images illustrates significant differences in the redox ratio between the different cell lines under normoxic conditions, and within each cell line after exposure to acute hypoxia (except 168FARN). Error bars represent standard deviation of the mean plate value. C. The normalized oxygen consumption rate (calculated as oxygen consumption rate/proton production rate) for all four cell lines and the direction of change after exposure to acute hypoxia are consistent with the optical redox ratio. Asterisks placed above bars indicate statistical significance. *** denotes $p < 0.0001$ and ** denotes $p < 0.01$.

Biomedical Optics EXPRESS

3.3 Reoxygenation following acute hypoxia leads to metastatic potential-dependent changes in the optical redox ratio

To determine if the metabolic response of each cell line following reoxygenation from acute hypoxia correlated with metastatic potential, we calculated the difference in redox ratio between the post-hypoxia and normoxia groups for each cell line. The metastatic 4T1 cells showed the largest increase in redox ratio following reoxygenation from acute hypoxia (Fig. 3). Statistical analysis using a two-factor nested ANOVA design showed that that the interaction between the two fixed effects - cell line and hypoxic perturbation – was statistically significant ($p < 0.0001$), demonstrating that reoxygenation from acute hypoxia had a significant, cell line-specific effect on the redox ratio. Furthermore, our data indicate that the cell line-specific changes showed a trend with metastatic potential.

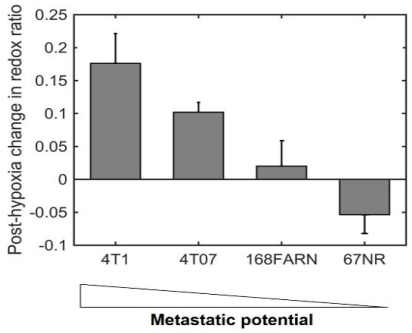

Fig. 3. Exposure to acute hypoxia leads to cell-line-dependent changes in redox ratio. Bar plots represent the difference in the mean values of normoxia and post-hypoxia reoxygenation groups. Error bars represent the standard deviation and were calculated as follows: $\sqrt{(sd_1)^2+(sd_2)^2}$, where sd_1 and sd_2 represent the normoxia and post-hypoxia groups within each cell line.

4. Discussion

Recent investigations of the link between metabolism and metastasis have determined that both oxidative phosphorylation and aerobic glycolysis play key roles at different stages of tumor growth, invasion, and metastasis. Due to its ability to report on the relative contributions of oxidative phosphorylation and glycolysis, the optical redox ratio presents a powerful method for determining cell metabolism and investigating the link between metabolism and metastasis. This preliminary study represents a first step towards determining the sensitivity of the optical redox ratio to metastatic potential in a controlled model of metastatic cancer progression.

To determine the sensitivity of the redox ratio to dynamic changes in oxygen consumption, we subjected 4T1 cells to the same metabolic perturbations as a standard Seahorse assay. Although the direction of change in the redox ratio in response to each drug was consistent with the Seahorse data, there was greater variance in our data compared with the Seahorse assay. This variance is likely due to experimenter error in drug delivery to the cells while placed under the microscope objective, which may have affected the homogeneity of distribution over the entire coverslip. On the other hand, drug injections and oxygen sensing are optimized in the Seahorse instrument. Data shown in Fig. 2 represent single time point measurements with no added drugs and show similar variance to the Seahorse results. The advantage of multiphoton microscopy lies in is its ability to provide spatial information that allows quantification of metabolic heterogeneity within cell populations and tumor organoids [34, 35]. Furthermore, multiphoton microscopy provides the ability to image deeper within tissue and investigate metabolic changes at different stages of the invasion-metastasis cascade in pre-clinical models of breast cancer.

Biomedical Optics EXPRESS

In addition to significant differences in the redox ratios between cell lines, we observed a trend towards higher redox ratio with increasing metastatic potential (168FARN<4T07<4T1), indicating a shift towards more mitochondrial oxidative metabolism. These data are consistent with studies showing enhanced oxidative phosphorylation in highly metastatic cells [8, 10]. Other researchers have found a higher redox ratio in highly aggressive MDA-MB-231 cells compared with the indolent MCF-7 cells [22, 26]. Ostrander et al. found that aggressive, triple-negative breast cancer cells had higher redox ratios compared with ER + breast cancer cells based on our definition of FAD/(FAD + NADH) [21]. Li and colleagues have shown a linear correlation between the redox ratio and invasive potential of melanoma xenografts [36].

Contrary to the trend of lower redox ratio with decreasing metastatic potential, the 67NR cells had a significantly higher redox ratio. Metabolomic analysis of the same panel of cell lines has shown that both glycolysis and Krebs cycle metabolites were abundant in the metastatic cell lines (4T07, 4T1, and 168FARN) whereas only glycolytic metabolites were found to be abundant in the non-metastatic 67NR cell line [8]. Therefore, we would expect the 67NR cells to have a lower redox ratio than the 168FARN cells. The increased redox ratio can be explained by a recent report indicating that the 67NR cells have significantly lower levels of succinate dehydrogenase (SDH) compared with 4T1 cells [29]. Lower levels of SDH lead to an accumulation of succinate and restricted metabolite flux through the Krebs cycle. Because FAD associated with succinate is not a significant contributor to overall FAD fluorescence [37], the increased redox ratio is likely due to reduced NADH generation due to restrictions in metabolite flux through the Krebs cycle. The increased redox ratio in the 67NR cells is also consistent with Seahorse assay measurements. The Seahorse metric that we used (n-OCR) represents the ratio of oxygen consumption rate (OCR) to proton production rate (PPR). Analyzed individually, both the OCR and PPR of 4T1 cells were approximately 3 times greater than the 67NR cells, consistent with other reports [11, 29]. This likely led to the n-OCR ratio being fairly similar between the two cell lines. The 67NR data seem to indicate, based on a limited sample size, that the baseline redox ratio itself has limited utility as a biomarker of metastatic potential. However, further studies using more breast cancer cell lines will be necessary to identify the utility of the baseline redox ratio as compared to the redox ratio in response to stress.

To elicit a further difference between these cell lines, and especially due to the similar redox ratios of 4T1 and 67NR, we subjected the cells to a hypoxic ‘stress test’. We exposed the cells to an acute hypoxia protocol – an hour of hypoxia (0.5% O_2) followed by an hour of reoxygenation. The oxygen gas levels used in our study are accepted values to create hypoxic conditions *in vitro* [38]. The duration of hypoxia and reoxygenation was selected to mimic the periodic variations in oxygen levels experienced by cells *in vivo* [39]. Acute hypoxia has been attributed to irregular development of the tumor vasculature, leading to variations in red cell flux through the vessels and hence fluctuations in oxygen availability to cells [40]. The periodicity of such fluctuations has been measured to be on the order of minutes to days [40, 41]. Dai et al. demonstrated that a single exposure to 0.5, 1, or 2 hours of acute hypoxia followed by reoxygenation increased clonogenic survival, cell motility and invasion in pancreatic cancer cells [33], while chronic or a continuous period of hypoxia led to cell death and did not increase cell motility. Exposure to repeated cycles of acute or perfusion-limited hypoxia has been shown to increase the number of breast cancer stem cells [42], and lead to increased metastatic burden in pre-clinical rodent models [43, 44]. Furthermore, a gene signature based on cellular response to hypoxia-reoxygenation was found to have better prognostic potential in breast cancers compared with other gene expression signatures currently approved for use in the clinic [45].

The acute hypoxia stress caused a dramatic change in the redox ratio that was dependent on metastatic potential. The redox ratio increased significantly in the 4T1 and 4T07 cells in response to acute hypoxia. Previous investigations of myocardial ischemia and reperfusion have found a significant increase in the redox ratio during reperfusion following ischemia that

Biomedical Optics EXPRESS

exceeded baseline redox values [46]. The increased redox ratio was attributed to mitochondrial dysfunction and an inability to reduce FAD and NAD^+ during the Krebs cycle. However, our Seahorse metabolic assay showed no impairment of mitochondrial activity in the 4T1 or 4T07 cells after acute hypoxia. The increased redox ratio in the 4T1 cells likely reflects metabolic adaptability to external stresses, such as hypoxia and glutamine deprivation compared with 67NR cells [29]. Metabolic adaptability has been suggested as an important hallmark of cells capable of successfully colonizing distant sites [47]. LeBleu et al. found that invasive breast cancer cells, such as 4T1 and MDA-MB-231 showed a significant increase in PGC-1α expression during reoxygenation from hypoxia, and that PGC-1α was responsible for increasing invasive potential by increasing oxidative phosphorylation [10]. The redox ratio decreased significantly in the 67NR cells during reoxygenation, a result that would typically be expected during hypoxic exposure. These results could indicate an inability of the 67NR cells to efficiently switch to oxidative phosphorylation during reoxygenation following acute hypoxia, thereby indicating a lack of invasive capabilities. Further studies using gene knockout models that eliminate cell migration and metastasis will be necessary to fully characterize the relationships between redox state, hypoxia, and migration. Additional studies to determine if non-metastatic 67NR tumors exposed to frequent episodes of acute hypoxia are able to generate metastatic nodes would provide an excellent model to understand the role of metabolism in driving tumor metastases.

In summary, we have identified metastatic potential-dependent differences in the redox ratio in a panel of isogenic breast cancer cell lines. Subjecting these cells to a stress test revealed greater metabolic adaptability in highly metastatic cells compared with non-metastatic cells. Measuring metabolic adaptability using a stress protocol could potentially reveal the metastatic capabilities of a cell. Because these results are based on triple-negative breast cancer cells, further studies are necessary to identify whether these metastatic potential-dependent changes are also seen in other types of cells, such as ER + and HER2 + breast cancer cells. Additionally, these data will need to be compared to current FDA-approved methods to determine risk of recurrence, such as Oncotype DX to enable clinical translation.

5. Appendix: effect of mitochondrial inhibitors and uncouplers on redox ratio

The sensitivity of the redox ratio to dynamic changes in oxygen consumption was evaluated using mitochondrial perturbations. The effects of these drugs on specific components of the electron transport chain and hence the redox ratio are illustrated in greater detail in Fig. 4.

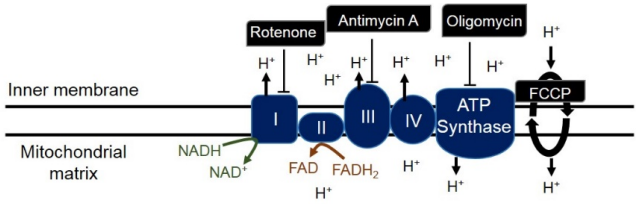

Fig. 4. Effect of mitochondrial inhibitors and uncouplers on redox ratio. Initial addition of oligomycin inhibits ATP synthase, which decreases mitochondrial respiration, increases NADH that cannot be converted to NAD^+ and hence decreases the redox ratio. FCCP is a mitochondrial uncoupler that causes protons to leak across the membrane, leading to a loss of proton gradient and hence the ability to generate ATP. Because the cell tries to restore the proton gradient, NADH is consumed, leading to increased redox ratio. Finally, Rotenone and Antimycin inhibit complexes I and III, leading to a shutdown of mitochondrial respiration and a decrease in the redox ratio.

Funding

National Institutes of Health (R00EB017723, R15CA202662) and University of Arkansas College of Engineering (ERISF seed grant).